MAP kinase and autophagy pathways cooperate to maintain RAS mutant cancer cell survival

Chih-Shia Lee[a], Liam C. Lee[a,g], Tina L. Yuan[b,h], Sirisha Chakka[c,i], Christof Fellmann[d,j], Scott W. Lowe[d,e], Natasha J. Caplen[c], Frank McCormick[b,f,1], Ji Luo[a,1]

[a] Laboratory of Cancer Biology and Genetics, Center for Cancer Research, National Cancer Institute, Bethesda, MD 20892, USA.

[b] Helen Diller Family Comprehensive Cancer Center, University of California San Francisco, San Francisco, CA 94158, USA.

[c] Genetics Branch, Center for Cancer Research, National Cancer Institute, Bethesda, MD 20892, USA.

[d] Cold Spring Harbor Laboratory, Cold Spring Harbor, New York 11724, USA.

[e] Howard Hughes Medical Institute, and Department of Cancer Biology & Genetics, Memorial Sloan Kettering Cancer Center, New York, NY 10065, USA.

[f] Cancer Research Technology Program, Frederick National Laboratory for Cancer Research, Leidos Biomedical Research, Frederick, MD 21702, USA

[g] Present Address: Medical Affairs, Loxo Oncology, Stamford, CT 06901, USA.

[h] Present Address: Oncology Translational Research, Novartis Institute for Biomedical Research, Cambridge, MA 02139, USA

[i] Present Address: National Center for Advancing Translational Sciences, National Institutes of Health, Rockville, MD 20850, USA

[j] Present Address: Institute of Data Science and Biotechnology, Gladstone Institutes, San Francisco, CA 94158, USA.

[1] To whom correspondence may be addressed: Frank McCormick (frank.mccormick@ucsf.edu), Ji Luo (ji.luo@nih.gov).

Keywords: KRAS | RAF | MAPK | autophagy | siRNA

Supporting Information (SI)

SI Notes

Phenotypic gap between targeting the KRAS oncoprotein itself versus its downstream effector network

Our analysis revealed a significant phenotypic gap between targeting the KRAS oncoprotein itself versus targeting its downstream effector network. We noted that none of the siRNA combinations could fully phenocopy *KRAS* knockdown: the best effector combination we identified only captures a little over 50% of *KRAS* dependency. Several explanations could be offered here. First, we might have missed better target combinations due to our limited sampling of the combinatorial space (~500 single nodes, node pairs and paralog combinations sampled out of all 1.82×10^9 possible combinations). Second, in the current study we did not analyze distal RAS effectors such as the ETS, FOS and FRA1 transcription factors (1-3) and other stress response pathways known to functionally interact with *KRAS* mutation (4-8). Thus, expanding the analysis to include these genes and pathways in a greater number of combinations could yield a more comprehensive landscape of pathway dependencies in *KRAS* mutant cells. Third and as discussed above, the heterogeneity nature of pathway dependency amongst *KRAS* mutant cell lines could imply that no public combination is able to effectively capture all of *KRAS* dependency across all cell lines. Finally, it is possible that the functional overlap between oncogenic and physiological RAS signaling imposes a selectivity ceiling. Thus, targeting KRAS onco-effectors may never achieve the same therapeutic window as targeting the KRAS oncoprotein itself. Recent efforts in developing novel $KRAS^{G12C}$ inhibitors have gained significant traction (9-11), a useful future direction would be to identify KRAS onco-effectors that strongly synergize with $KRAS^{G12C}$ inhibitors to enhance the genotype-dependent killing of *KRAS* mutant cancer cells.

SI Materials and Methods

RAS effector and stress pathway gene siRNA library curation details

Sensor siRNAs against the list of RAS effector genes interrogated in this study were generated as previously described (12, 13). Briefly, 65 bioinformatically predicted potent shRNA sequences against each gene were functionally analyzed using the Sensor assay (12) and the top 5 most potent Sensor shRNA sequences were converted to 22-mer Sensor siRNA sequences. From these, the top 2 most potent Sensor siRNAs that work in a pool format were identified as follows. Candidate siRNAs each targeting a different gene were mixed in a pool of 4-6 siRNAs and co-transfected into human osteosarcoma U-2 OS cells for 72h. U-2 OS cells were relatively insensitive to RAS pathway gene knockdown. In addition, we took advantage of gene paralog redundancy during this validation step to minimize toxicity of siRNA pools to U-2 OS cells. To maximize assay sensitivity and minimize siRNA off-target effects, each siRNA was tested at a low 2nM transfection concentration (13). Total RNA was first isolated using the RNeasy Mini Kit (Qiagen #74106), reverse-transcribed into cDNA using the High Capacity cDNA Reverse Transcription Kit (Applied Biosystems #4368814), and then subjected to RT-qPCR reaction (Applied Biosystems 7900HT Fast Real-Time PCR System) for measuring the knockdown efficiency of each target mRNA. *GAPDH* mRNA was used as a normalization control. A Sensor siRNA would qualify and be curated into our library when its knockdown efficiency is > 70%. For the rare instances where we were unable to qualify two independent Sensor siRNAs, commercially available siRNAs (Qiagen) were included in the validation pipeline and the knockdown threshold was lowered to 65%. For each target gene, its most potent siRNA was assigned to the Set 1 library and the second most potent siRNA was assigned to the Set 2 library. For a selected subset of on-target siRNAs in our library, we generated their sequence-specific C911 rescue siRNAs by changing bases 9, 10, and 11 of the guide strands to their complement bases as previously described (14). These C911 siRNAs abolish RISC-mediated on-target mRNA cutting but preserve seed sequence-mediated, miRNA-like off-target effects. All siRNA sequences used in the present study are listed in Dataset S1.

Cell lines and cell culture media detailed information

Human colorectal cancer cell lines DLD-1, HCT116, SW620, LoVo, SW403, SW48, and Caco-2 were cultured in McCoy's 5A media (Lonza #12-688F) supplemented with 10% fetal bovine serum (Gibco #10438026). Human pancreatic ductal adenocarcinoma cell lines MIA PaCa-2, HUP-T4, SUIT-2, AsPC-1, PA-TU-8902, and BxPC-3 cells were cultured in RPMI 1640 media (Lonza #12-167F) supplemented

with 10% fetal bovine serum. Cell lines were authenticated by short-tandem repeat profiling (Laragen, Inc). Human mammary epithelial cells (HMEC) were cultured in MEGM media with supplements (Lonza # CC-4136). Immortalized human small airway epithelial cells (iSAEC) were previously described (15) and were cultured in SAGM media with supplements (Lonza #CC-3118). Human pancreas duct normal epithelial cells (HPNE) were cultured in mixture of 75% DMEM without glucose and glutamine (Gibco #A14430) and 25% M3:BaseF medium (Incell Cprporation #M300F-100) supplemented with 5% fetal bovine serum, 5.5 mM D-glucose (Gibco #A24940), 2 mM L-glutamine (Lonza #17-605E), 10 ng/ml recombinant human EGF (Gibco #PHG0311L), and 750 ng/ml puromycin (Gibco # A1113803). Human BJ fibroblast cells were cultured in EMEM (ATCC #30-2003) supplemented with 10% fetal bovine serum. All cell lines were cultured at 37 °C in a humidified 5 % CO_2 incubator.

Reverse transfection of siRNA combinations and co-treatment with siRNAs and inhibitors

To knockdown multiple gene targets simultaneously, reverse siRNA transfection was performed using a protocol similar to a previous study (16) with modifications. Briefly, 2 µl of each siRNA pool was first arrayed in 384-well tissue culture plates (Corning #3570) and stored at -80C until used. The siRNA concentration was adjusted in the pool such that the final concentration for each individual siRNA in the pool during the transfection step was 5nM. Depending on the specific siRNA combination, up to 6 siRNAs were combined together in each pool. To maintain consistency during the siRNA transfection step, the total siRNA concentration was kept at a constant 30 nM: if fewer than six siRNAs were included, negative control siRNA (Qiagen AllStars Negative Control siRNA, #SI03650318) was added to the siRNA pool to bring total siRNA concentration to 30 nM.

For the transfection reaction, negative control siRNA at 30nM was included for non-specific transfection toxicity. A lethal siRNA pool, siDeath, (Qiagen AllStars Human Cell Death Control siRNA, # SI04381048) was included at a concentration gradient of 2.5, 5, 10, and 30 nM as the positive control to monitor transfection efficiency. For the transfection reaction, Lipofectamine RNAiMAX (Invitrogen # 13778150) was diluted in 20 µl McCoy's 5A or RPMI 1640 base media without supplements and dispensed into wells containing pre-arrayed siRNAs. Cell suspension was prepared in culture media supplemented with 20% FBS, and 20 µl of cell suspension was then dispensed into each well and mixed with the lipid and siRNA complex. Lipid concentration and the cell number were optimized for each individual cell line to obtain minimal toxicity with negative control siRNA and maximum toxicity with lethal positive control siRNAs.

For siRNA and inhibitor co-treatment, cells were transfected with siRNA mixtures first. Five microliters of inhibitors were added into culture 24 hr post-siRNA transfection such that the desired drug concentrations were reached in the media. Dose response curves were modeled for determining IC_{50} values by using GraphPad Prism software (GraphPad Software).

Cell viability, caspase 3/7 activity, and cell cycle assays. To examine the effect of siRNA-mediated gene knockdown on cell viability and apoptosis, cell viability was measured 5 days post-transfection using ATP-based CellTiter-Glo Luminescent Cell Viability Assay (Promega #G8462). To examine the effect of siRNA-mediated gene knockdown on apoptosis, cells at 3-days post transfection were analyzed for caspase 3/7 activity using ApoLive-Glo Multiplex Assay (Promega #G6411). In this assay, cell viability was first measured with a fluorescence-based, non-cell lytic assay. Caspase 3/7 activity was then measured by a lytic, luminescence-based assay, and adjusted by the corresponding viability obtained from the first part of the multiplex assay. To compare the effect of different siRNA pools within and across experiments, cell viability and apoptosis was normalized to in-plate negative control siRNA wells. Cell cycle analysis was performed as previously described (17). Briefly, cells were transfected with siRNA pools in 6-well plates. At 3 days post transfection, both floating cells and attached cells were harvested, fixed in 70% ice-cold ethanol, treated with RNase A and stained with propidium iodide. Cell cycle distribution was analyzed by flow cytometry using a FACSCantoII instrument with the FACSDiva software (Becton Dickinson). Cell cycle distribution was analyzed using the ModFit LT v5.0 software (Verity Software House). Cell fractions in G_0/G_1, S, and G_2/M phases were determined using the viable cell population; whereas the sub-G_1 fraction was determined using the total cell population.

Immunoblotting. To examine the effect of siRNA-mediated knockdown on protein expression and pathway activity, cells were reversely transfected with siRNA pools in 96-well plates. At 5 days post-siRNA transfection, cell viability in each well was first determined using a non-lytic cell viability assay by performing CellTiter-Fluor Cell Viability Assay (Promega #G6082). Whole cell extract was harvested using Laemmli sample buffer with buffer volume adjusted in proportion to cell viability. Samples were subjected to SDS-PAGE followed by immunoblotting using primary antibodies from the following sources: KRAS (Sigma #WH0003845M1), ARAF (Santa Cruz Biotechnology #SC-408), BRAF (Santa Cruz Biotechnology #SC-5284), CRAF (BD Biosciences #610151), RAC1 (Cytoskeleton #ARC03), ATG7 (Cell Signaling #2631), phospho-MEK1/2_S217/S221 (Cell Signaling #9121), MEK1&2 (Cell Signaling #8727), phospho-ERK1/2_ T202/Y204 (Cell Signaling #9106), ERK1&2 (Cell Signaling #9102), phospho-FRA1_S265 (Cell Signaling #5841), FRA1 (Cell Signaling #5281),

BIM (Cell Signaling #2933), ATG5 (Cell Signaling #12994), LC3B (Cell Signaling #3868), p62 (Santa Cruz Biotechnology #SC-28359), and GAPDH (Santa Cruz Biotechnology #SC-47724). HRP-conjugated anti-rabbit and anti-mouse secondary antibodies were from Jackson Immuno Research. Immunoblots were imaged using a ChemiDoc Touch Imaging System (Bio-Rad) and chemiluminescence signal was quantified using the Image Lab Software (Bio-Rad). Analyte protein or phospho-protein level was normalized to GAPDH protein level in the same sample. Changes in total protein or phospho-protein level in response to siRNA was compared to sample transfected with negative control siRNA.

Data analysis and statistics. To assess the differential impact of siRNAs on *KRAS* mutant and WT cancer cell lines as well as immortalized, non-transformed normal cell lines, we first normalized cell viability in response to different siRNA pools to that of negative control siRNA for each individual cell line. Next, we quantified the effect of each siRNA pools using the following metrics. For each *KRAS* mutant cancer cell line, we calculated the differential dependency score (DDS) for each siRNA pool using *KRAS* WT cancer cell lines as the baseline: $DDS = \overline{V}_{WT} - v_{mut}$, where $\overline{V}_{WT}$ is the mean normalized viability of all *KRAS* WT cancer cell lines and v_{mut} is the normalized viability of the specific *KRAS* mutant cell line in response to an siRNA pool. For each *KRAS* mutant cell line, we also calculated the differential dependency score (DDSn) for each siRNA pool using normal cell lines as the baseline: $DDSn = \overline{V}_{norm} - v_{mut}$, where $\overline{V}_{norm}$ is the mean normalized viability of all normal cell lines and v_{mut} is the normalized viability of the specific *KRAS* mutant cell line in response to an siRNA or siRNA combination. To quantify the extent by which each siRNA pool captures *KRAS* dependency, its mean DDS and DDSn across *KRAS* mutant cell lines was compared to that of *KRAS* siRNAs. We also calculated the Pearson correlation coefficient (r) for an siRNA pool versus siKRAS using their viability data in *KRAS* mutant cell lines: $r = \frac{\sum_{i=1}^{n}(c_i-\overline{C})(k_i-\overline{K})}{\sqrt{\sum_{i=1}^{n}(c_i-\overline{C})^2}\sqrt{\sum_{i=1}^{n}(k_i-\overline{K})^2}}$, where c_i and $\overline{C}$ are the specific and mean normalized viability, respectively, of *KRAS* mutant cell lines in response to an siRNA or siRNA combination, and k_i and $\overline{K}$ are the specific and mean normalized viability, respectively, of *KRAS* mutant cell lines in response to siKRAS. Unsupervised hierarchical clustering was performed by using Partek Genomic Suite software (Partek Incorporated). Outlier analysis, paired *t*-test and ANOVA and post analysis were performed by using GraphPad Prism (GraphPad Software).

SI References

1. Tetsu O & McCormick F (2017) ETS-targeted therapy: can it substitute for MEK inhibitors? *Clin Transl Med* 6(1):16.
2. Monje P, Marinissen MJ, & Gutkind JS (2003) Phosphorylation of the carboxyl-terminal transactivation domain of c-Fos by extracellular signal-regulated kinase mediates the transcriptional activation of AP-1 and cellular transformation induced by platelet-derived growth factor. *Mol Cell Biol* 23(19):7030-7043.
3. Vallejo A*, et al.* (2017) An integrative approach unveils FOSL1 as an oncogene vulnerability in KRAS-driven lung and pancreatic cancer. *Nature communications* 8:14294.
4. Yu B*, et al.* (2015) Oncogenesis driven by the Ras/Raf pathway requires the SUMO E2 ligase Ubc9. *Proc Natl Acad Sci U S A* 112(14):E1724-1733.
5. Commisso C*, et al.* (2013) Macropinocytosis of protein is an amino acid supply route in Ras-transformed cells. *Nature* 497(7451):633-637.
6. Malone CF*, et al.* (2017) mTOR and HDAC Inhibitors Converge on the TXNIP/Thioredoxin Pathway to Cause Catastrophic Oxidative Stress and Regression of RAS-Driven Tumors. *Cancer Discov* 7(12):1450-1463.
7. Martin TD*, et al.* (2017) A Role for Mitochondrial Translation in Promotion of Viability in K-Ras Mutant Cells. *Cell Rep* 20(2):427-438.
8. Gwinn DM*, et al.* (2018) Oncogenic KRAS Regulates Amino Acid Homeostasis and Asparagine Biosynthesis via ATF4 and Alters Sensitivity to L-Asparaginase. *Cancer Cell* 33(1):91-107 e106.
9. Lito P, Solomon M, Li LS, Hansen R, & Rosen N (2016) Allele-specific inhibitors inactivate mutant KRAS G12C by a trapping mechanism. *Science* 351(6273):604-608.
10. Patricelli MP*, et al.* (2016) Selective Inhibition of Oncogenic KRAS Output with Small Molecules Targeting the Inactive State. *Cancer discovery* 6(3):316-329.
11. Xiong Y*, et al.* (2017) Covalent Guanosine Mimetic Inhibitors of G12C KRAS. *ACS Med Chem Lett* 8(1):61-66.
12. Fellmann C*, et al.* (2011) Functional identification of optimized RNAi triggers using a massively parallel sensor assay. *Mol Cell* 41(6):733-746.
13. Yuan TL*, et al.* (2014) Development of siRNA Payloads to Target KRAS-Mutant Cancer. *Cancer Discov* 4(10):1182-1197.
14. Buehler E, Chen YC, & Martin S (2012) C911: A bench-level control for sequence specific siRNA off-target effects. *PLoS One* 7(12):e51942.
15. Smith JL*, et al.* (2016) One-step immortalization of primary human airway epithelial cells capable of oncogenic transformation. *Cell Biosci* 6:57.
16. Garimella SV*, et al.* (2014) Identification of novel molecular regulators of tumor necrosis factor-related apoptosis-inducing ligand (TRAIL)-induced apoptosis in breast cancer cells by RNAi screening. *Breast Cancer Res* 16(2):R41.
17. Weng MT*, et al.* (2012) Evolutionarily conserved protein ERH controls CENP-E mRNA splicing and is required for the survival of KRAS mutant cancer cells. *Proc Natl Acad Sci U S A* 109(52):E3659-3667.

Lee et al. Figure S1

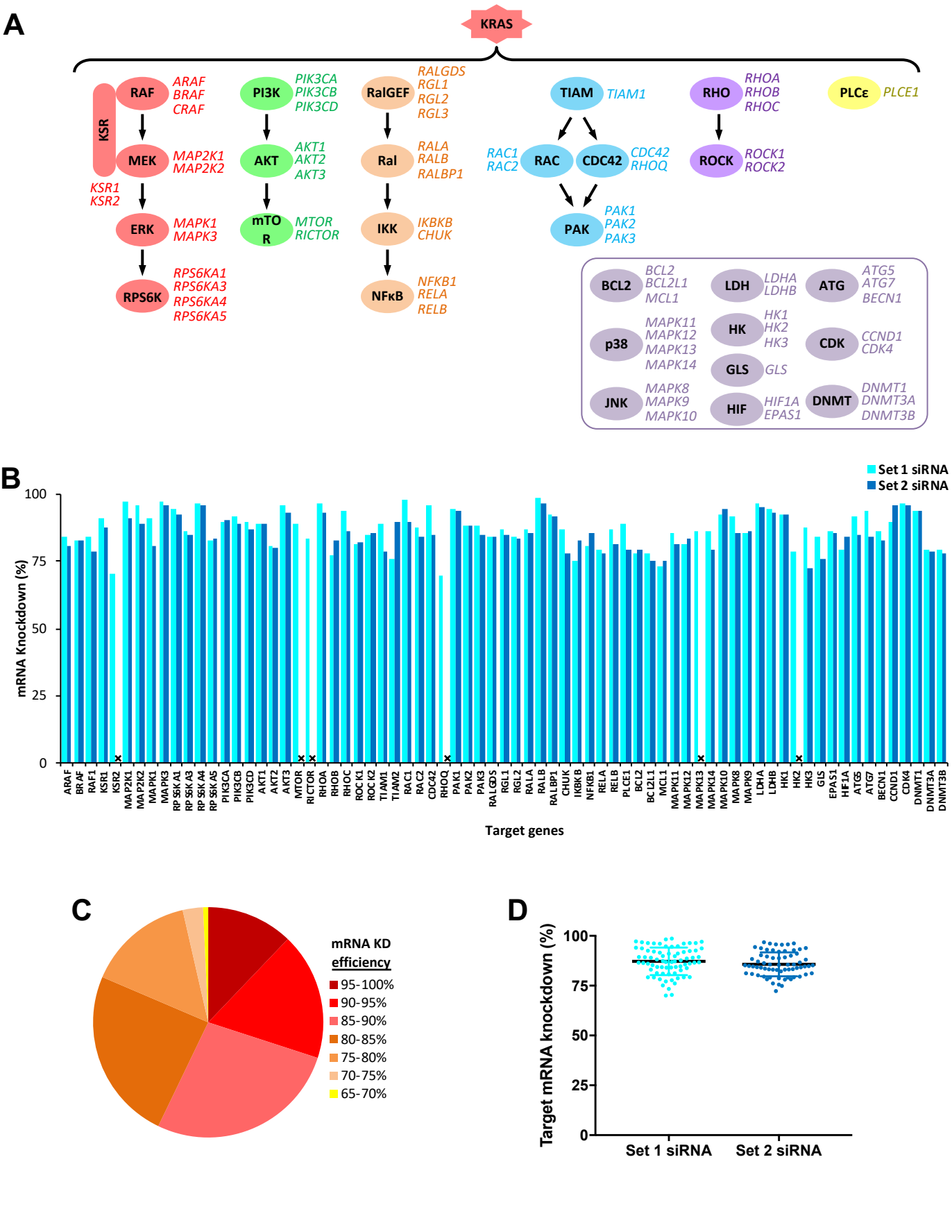

Lee et al. Figure S1 (cont.)

E

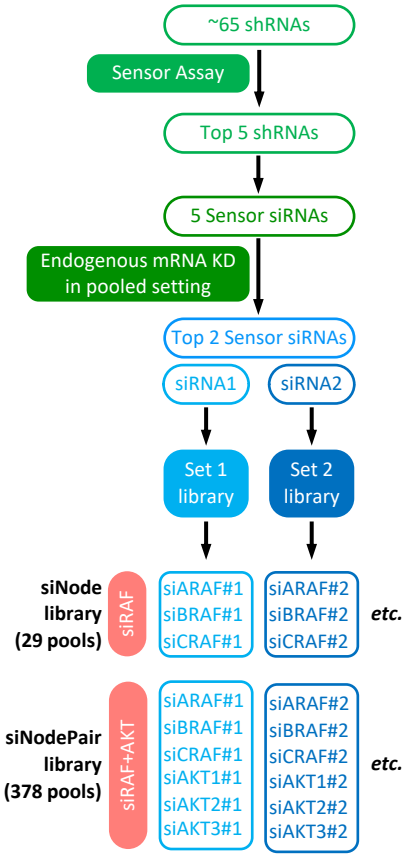

Lee et al. Figure S2

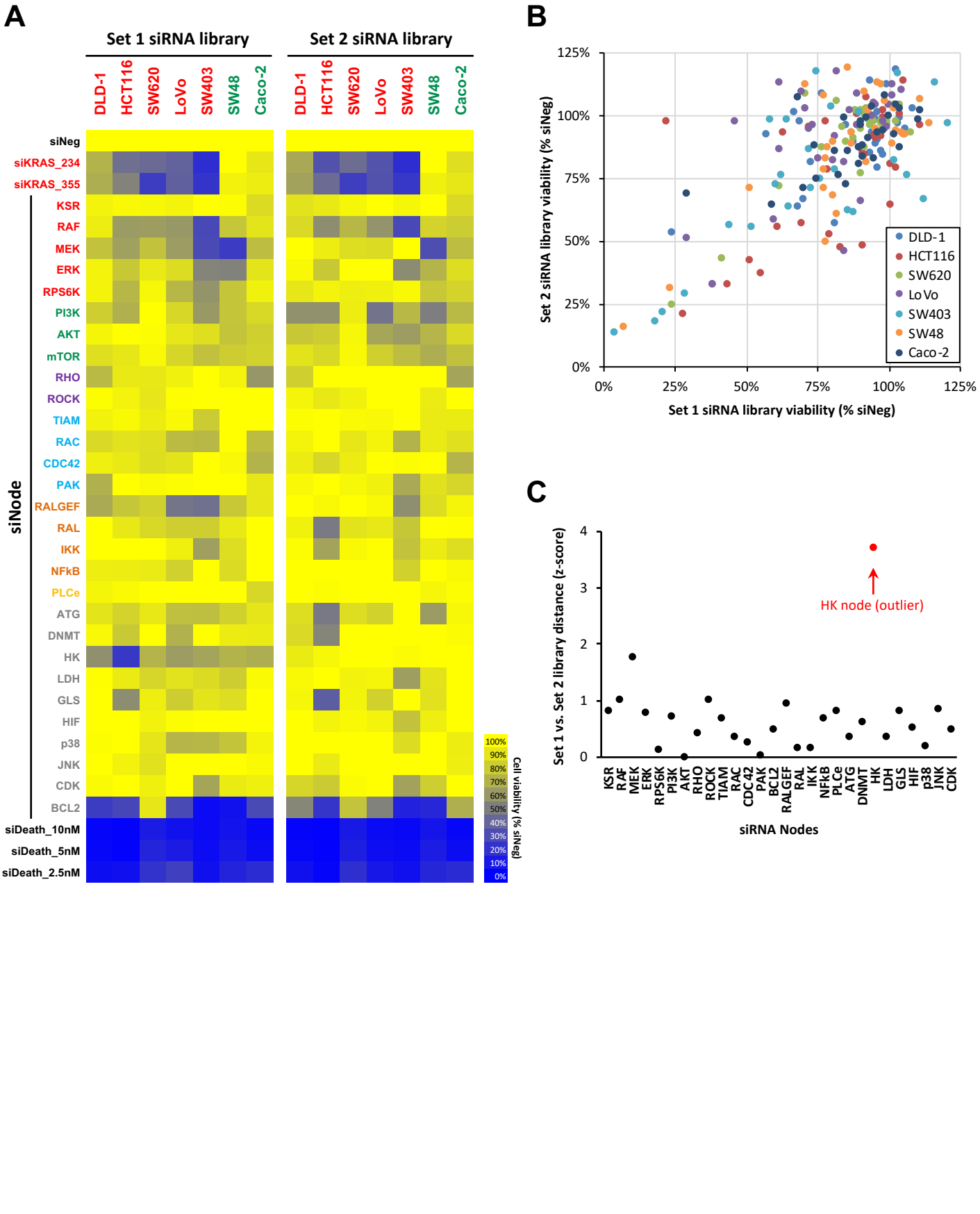

Lee et al. Figure S3

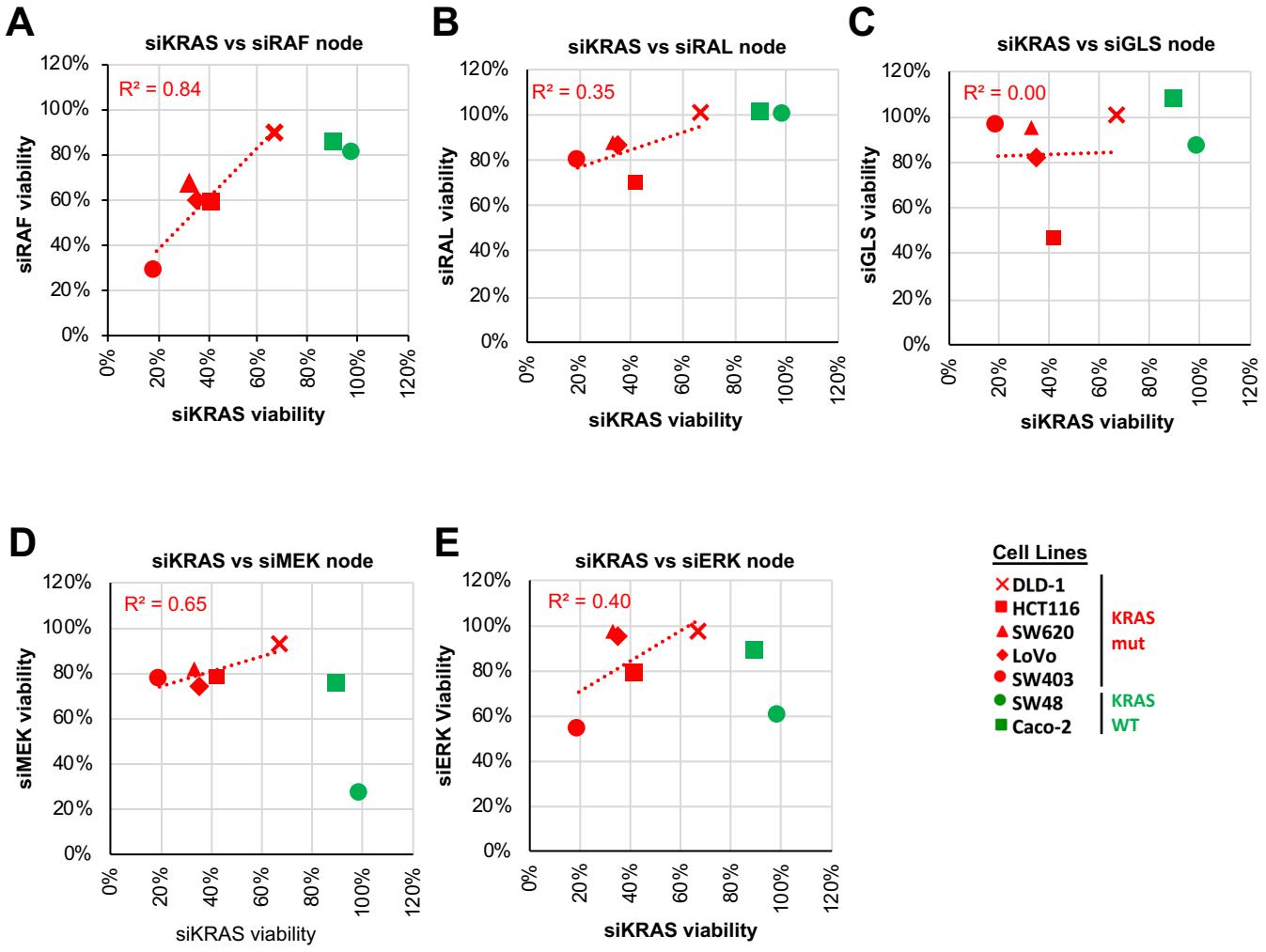

Lee et al. Figure S4

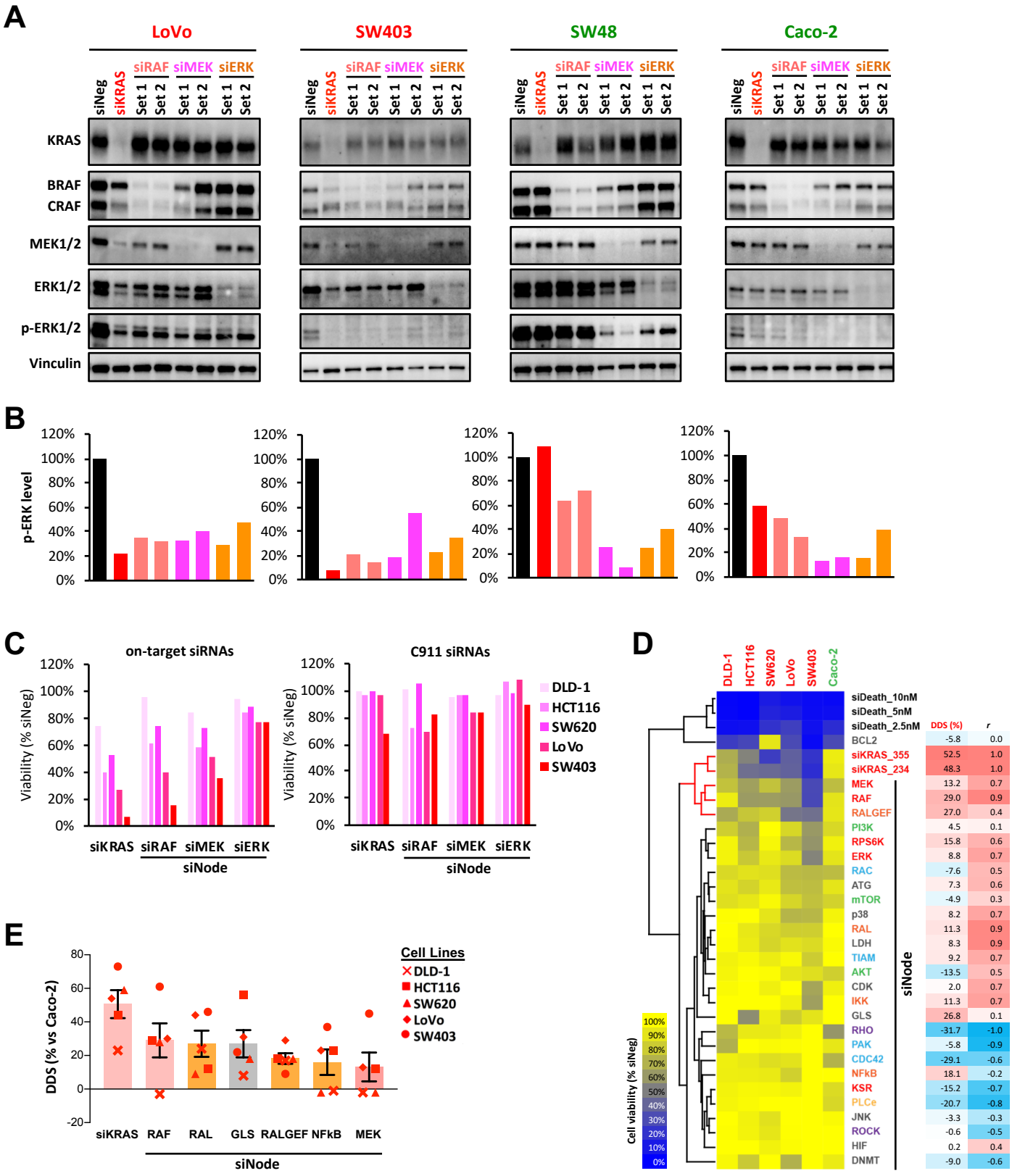

Lee et al. Figure S5

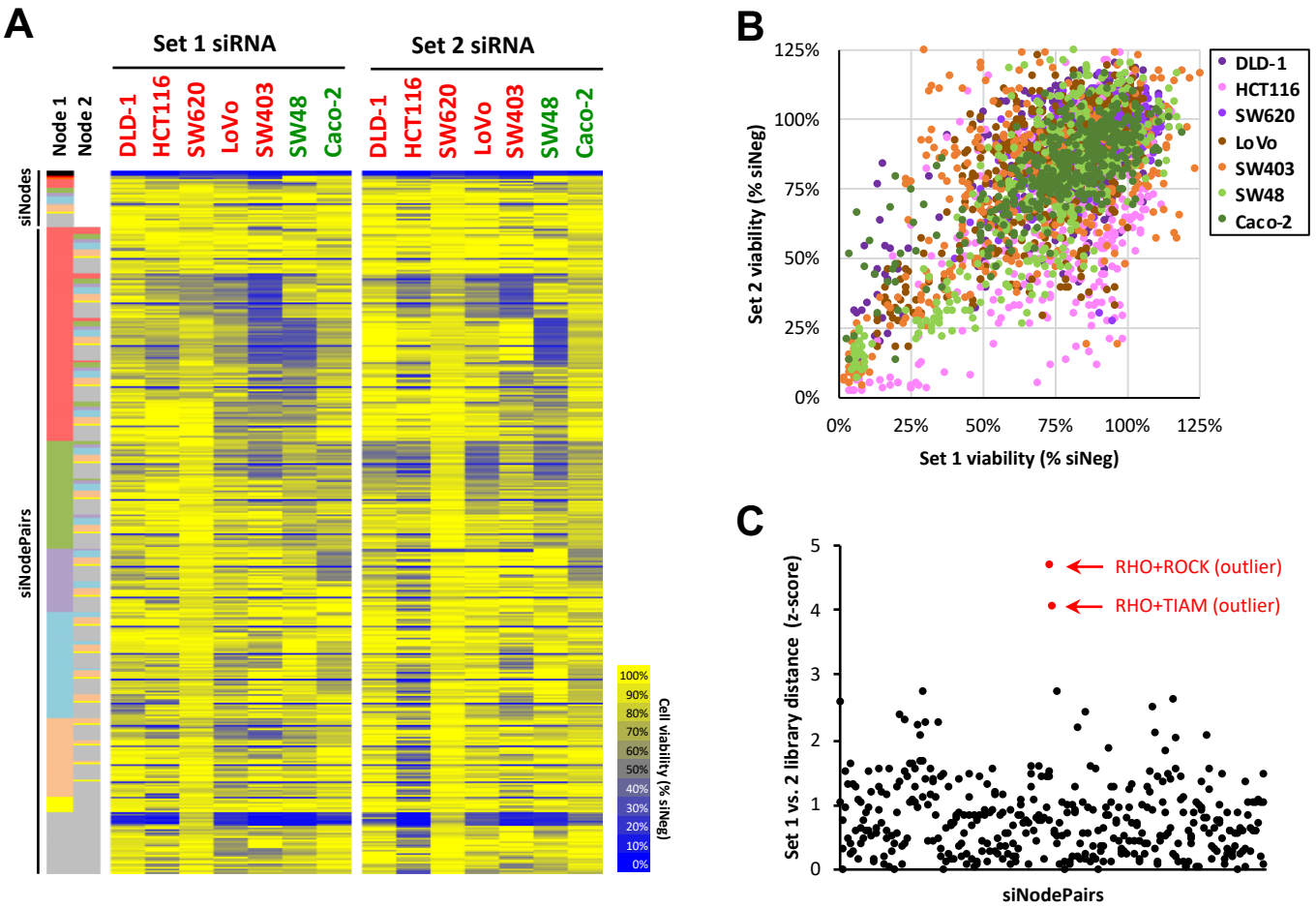

Lee et al. Figure S6

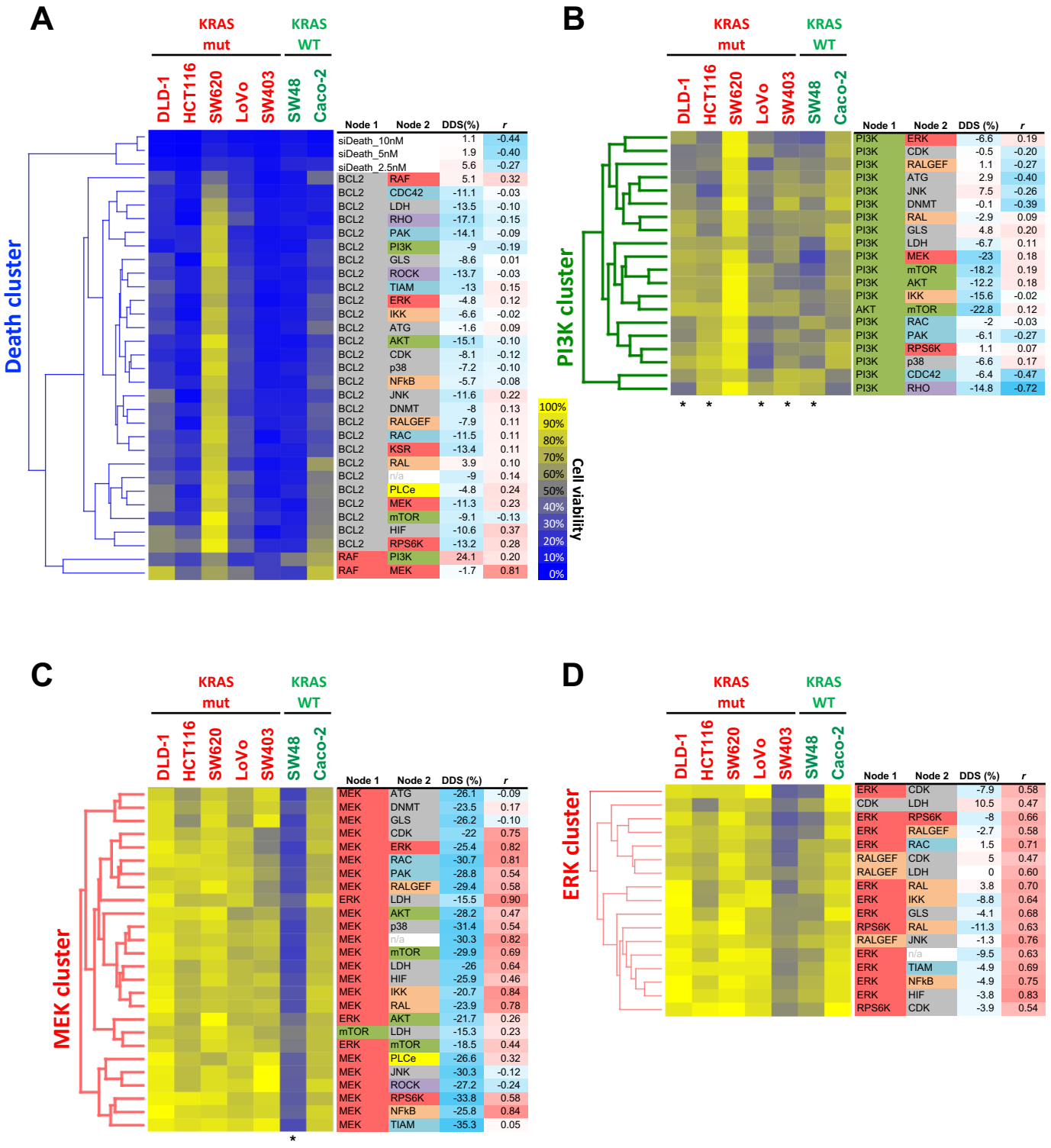

Lee et al. Figure S7

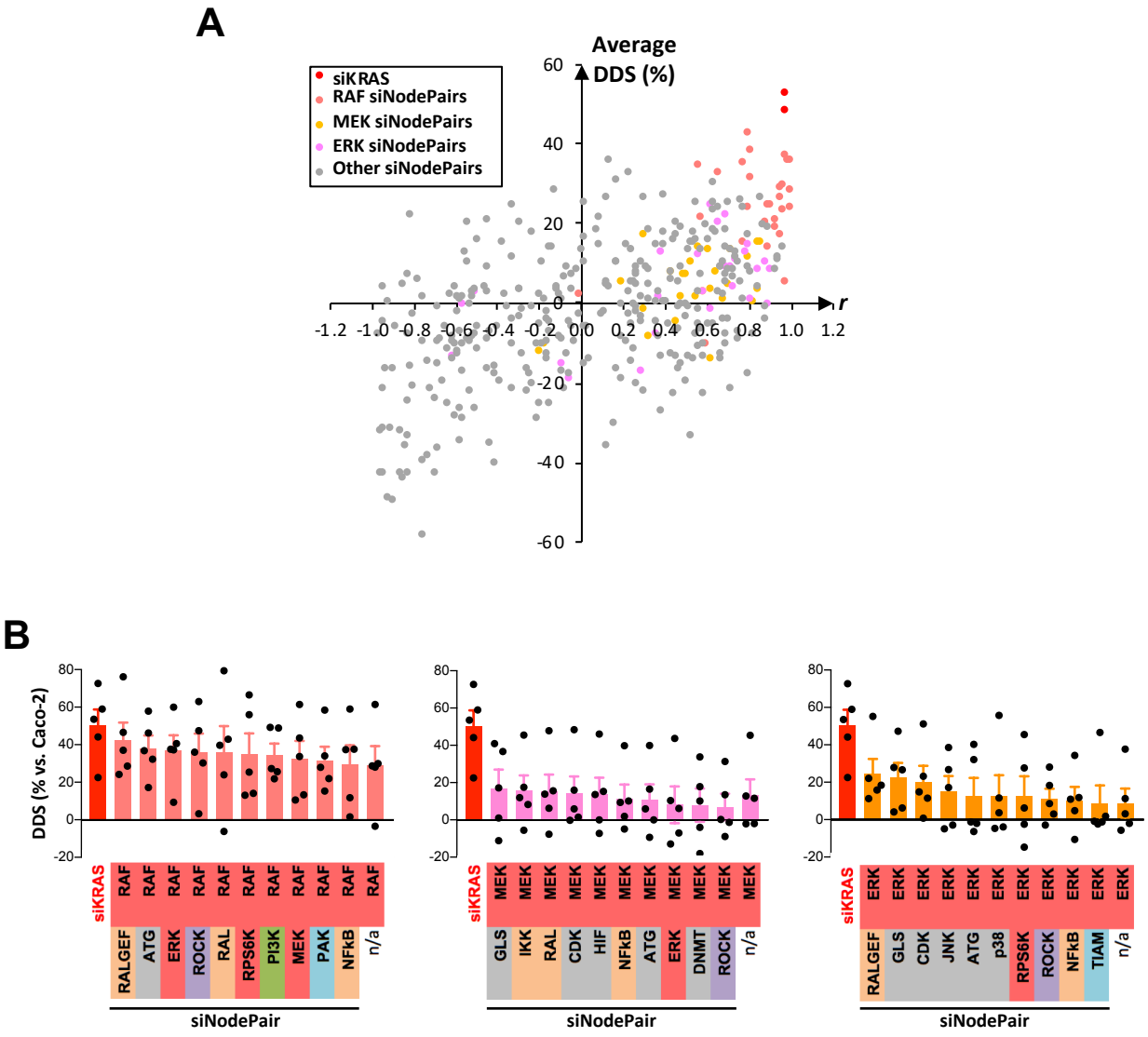

Lee et al. Figure S8

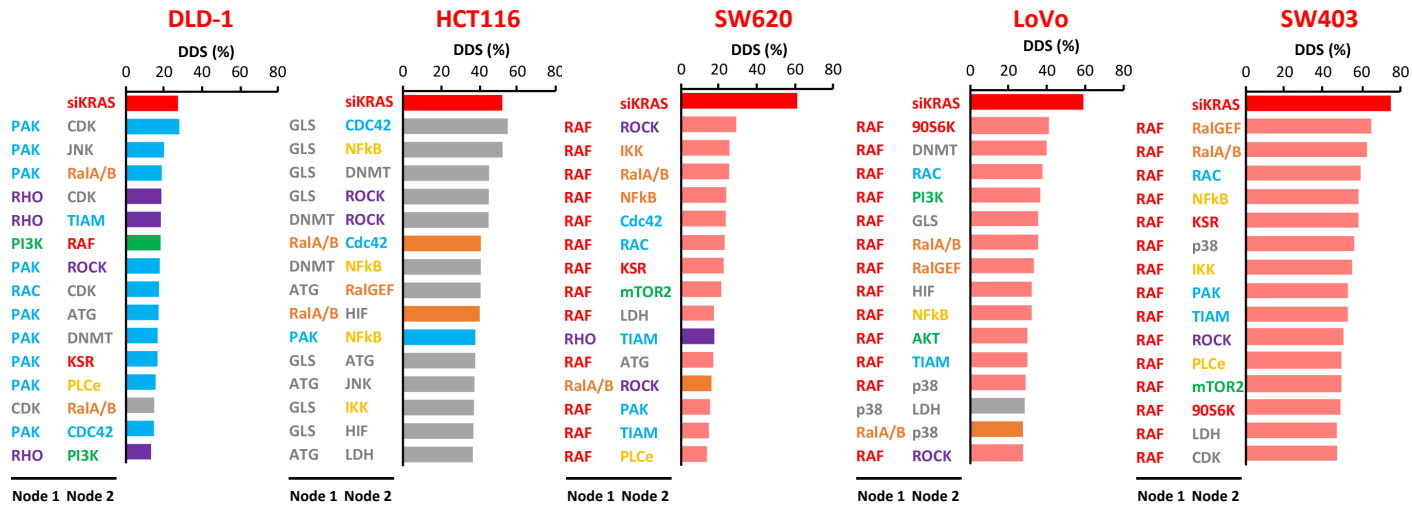

Lee et al. Figure S9

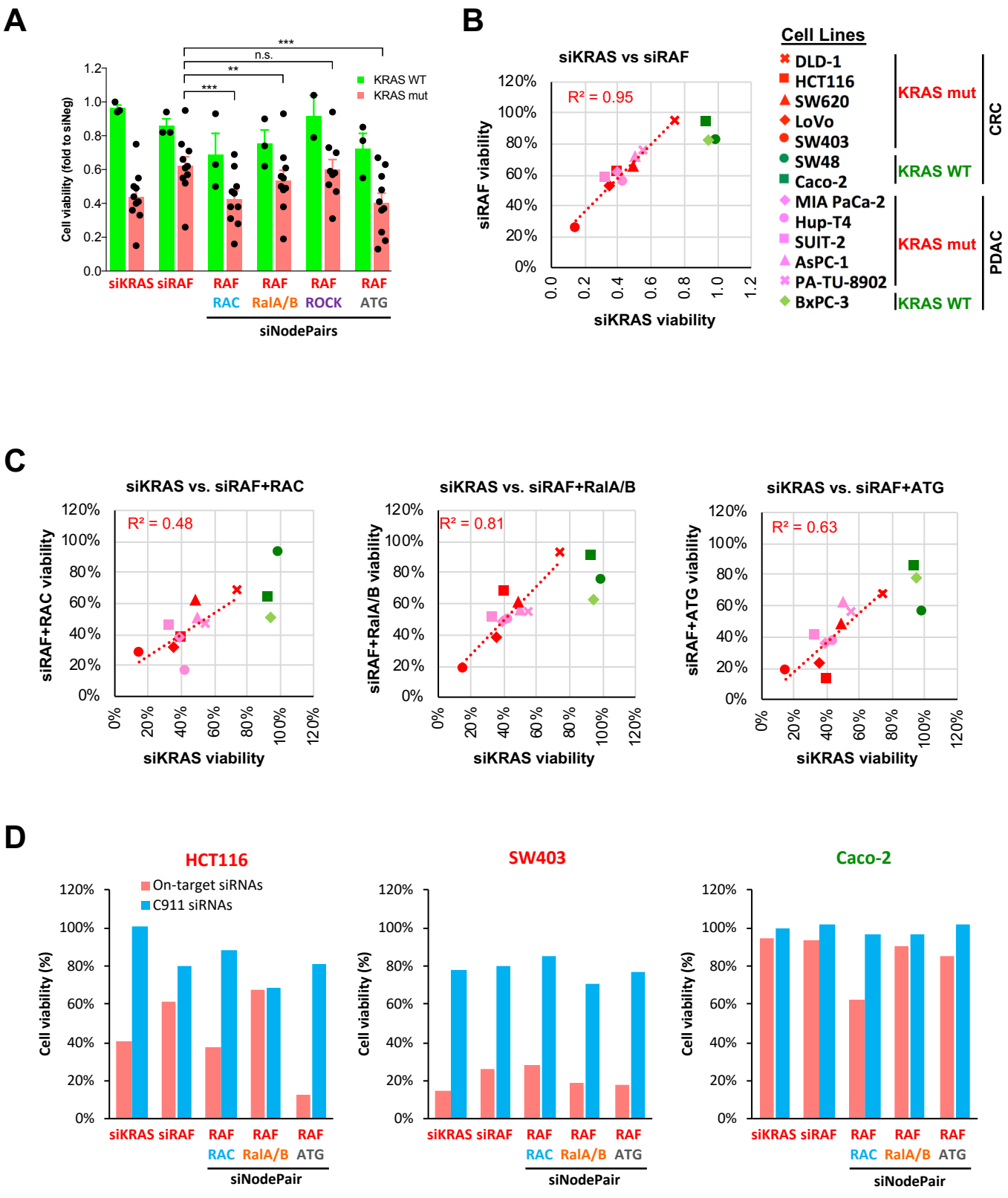

Lee et al. Figure S10

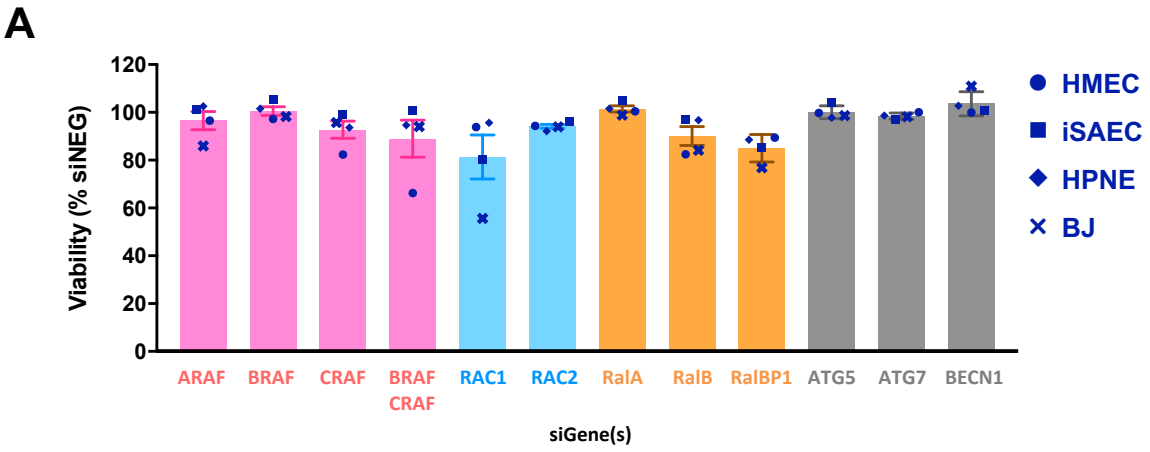

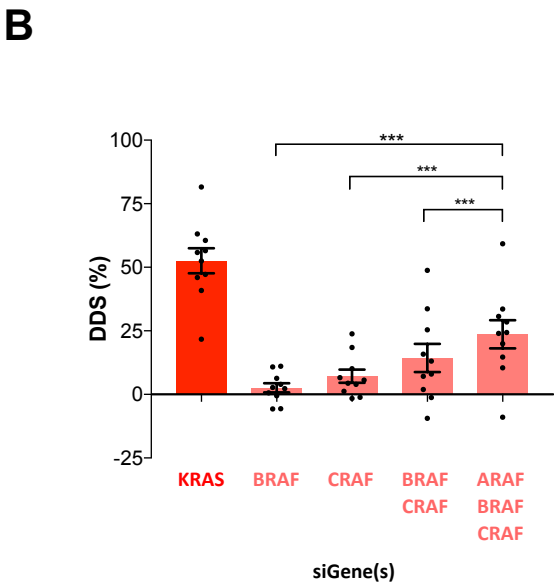

Lee et al. Figure S11

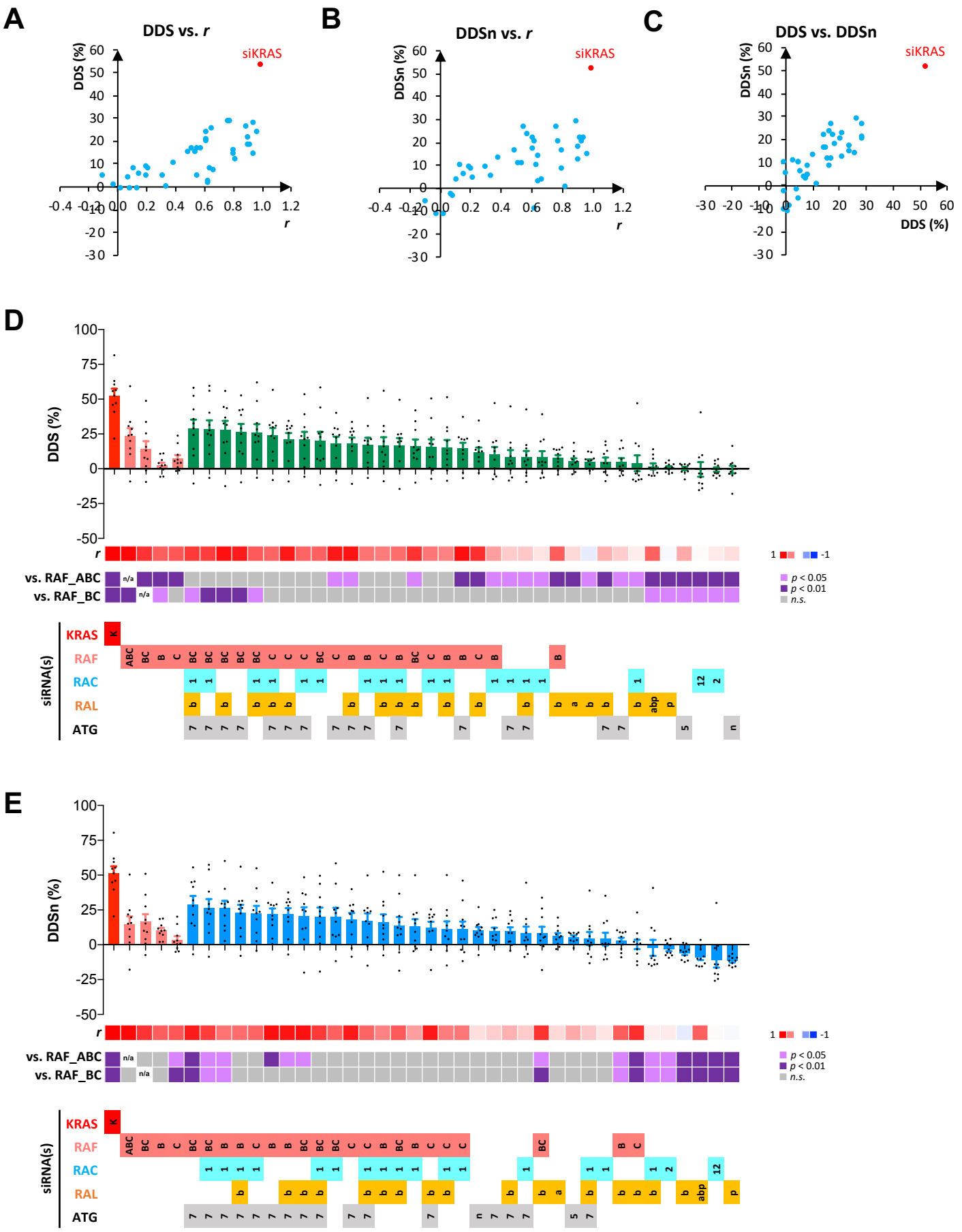

Lee et al. Figure S12

Lee et al. Figure S13

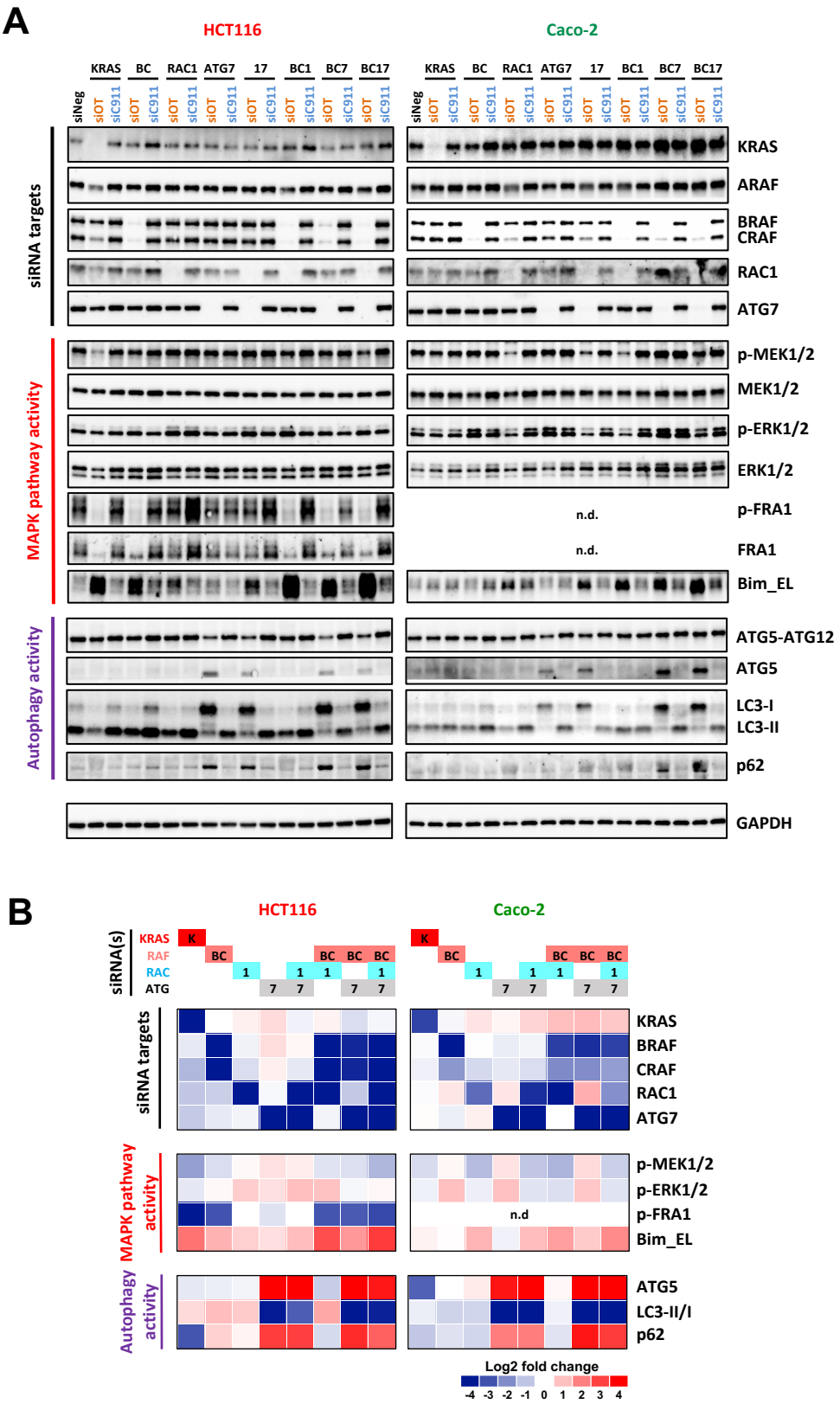

Lee et al. Figure S14

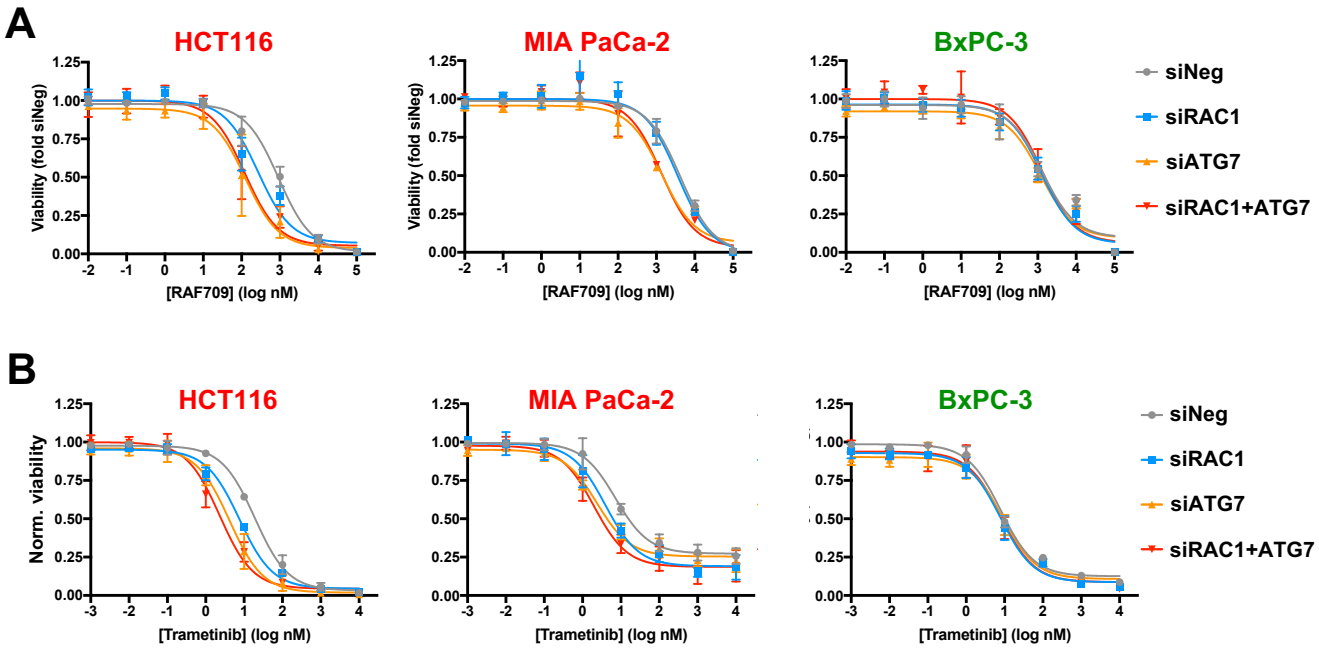

Lee et al. Figure S15

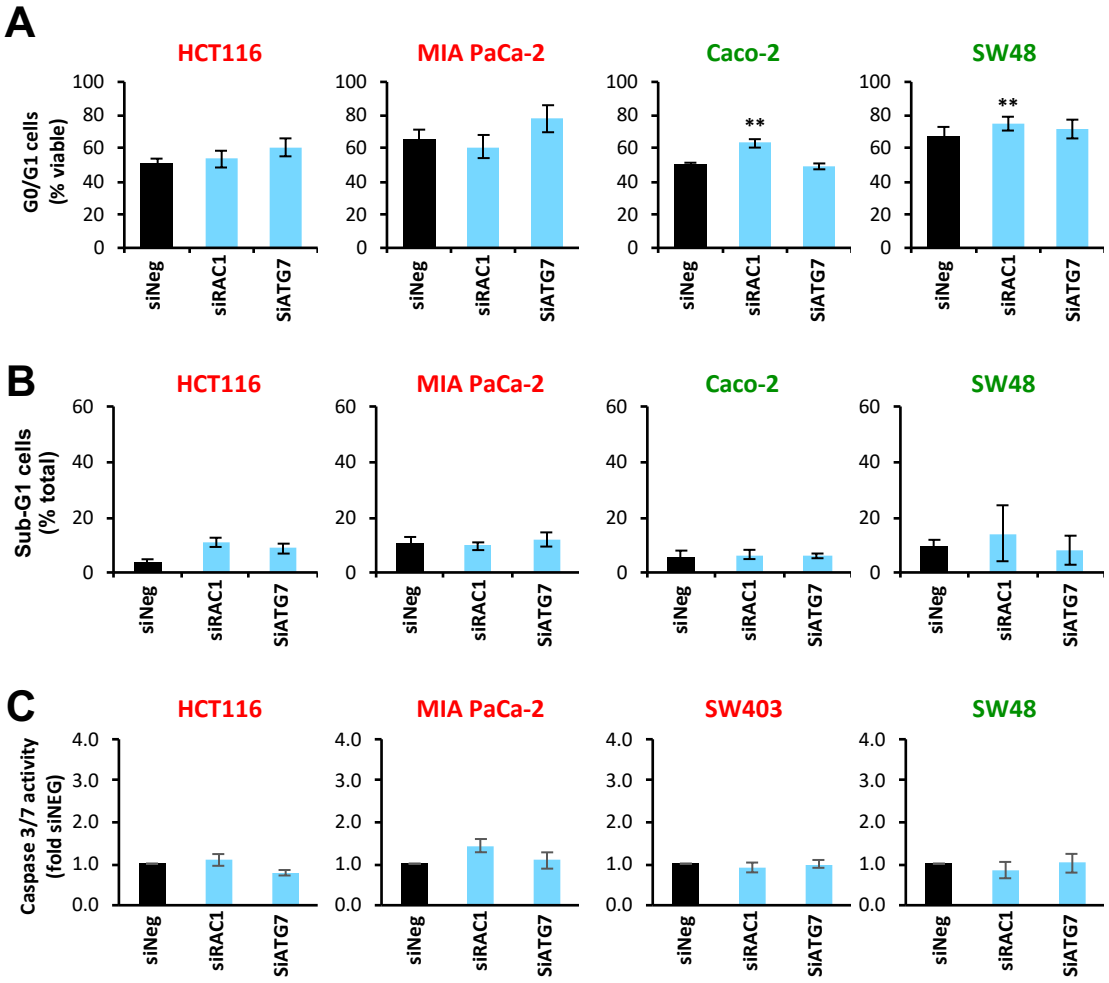

Lee et al. Figure S16

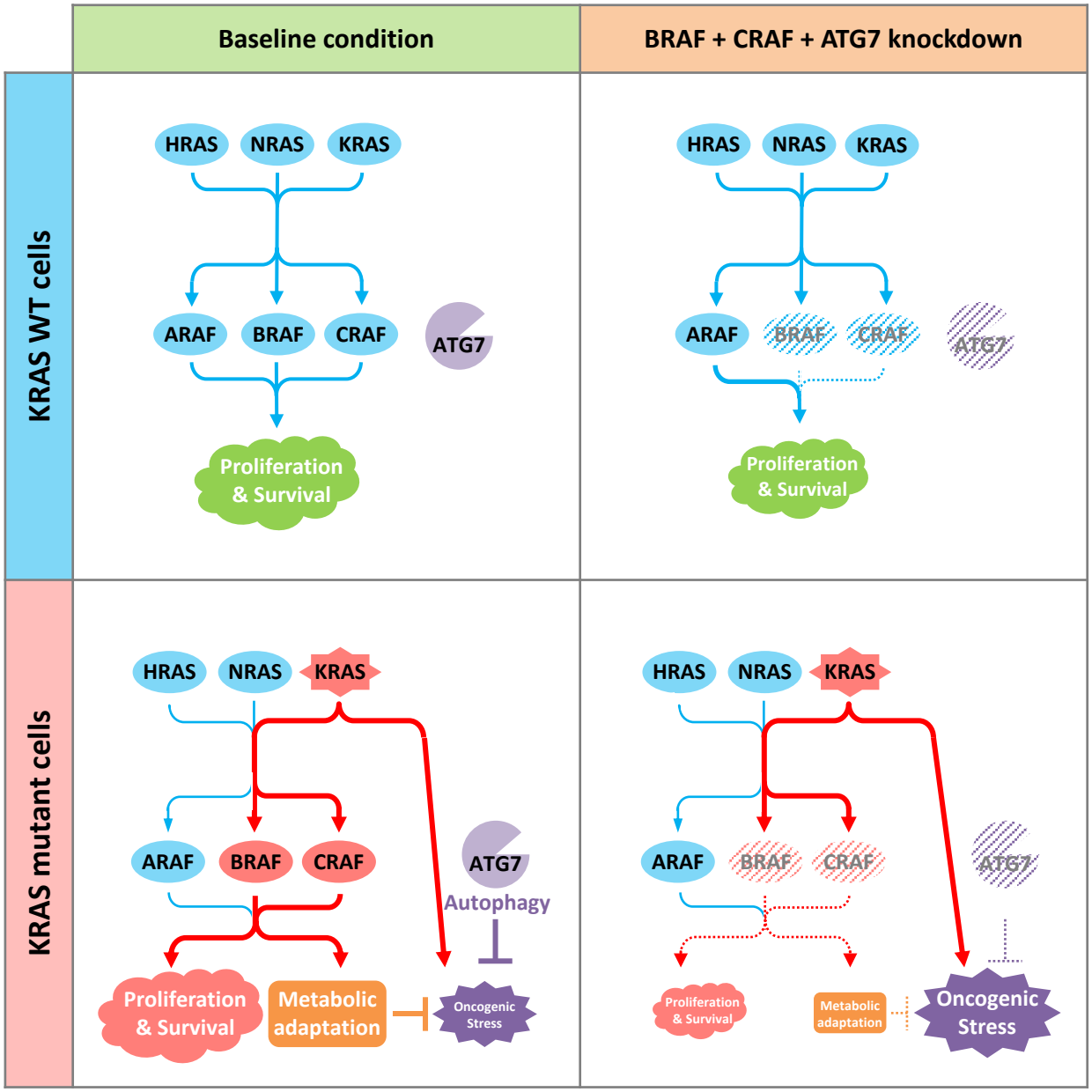

Supplemental Figure Legends

Fig. S1. Construction of an siRNA library targeting RAS effector and stress-response genes.

- **A.** Twenty-nine gene nodes from 6 canonical RAS effector pathways and 10 gene nodes from selected stress response and metabolic pathways (boxed) were included in our analysis. For each gene node, the gene paralogs are listed next to the node.
- **B.** Knockdown efficiency of the validated siRNAs in the library. Two Sensor siRNAs with target mRNA knockdown efficiency of > 70% in a pooled setting were included in the library. For each gene, the most potent siRNA was assigned to the Set 1 siRNA library and the second most potent siRNA was assigned to the Set 2 siRNA library. For six genes only one qualified siRNA was identified (× indicates no Set 2 siRNA was available), and the same siRNA was used in Set 2 library.
- **C.** Distribution of knockdown efficiency of all siRNAs included in the library.
- **D.** Comparison of knockdown efficiency of Set 1 and Set 2 library siRNAs.
- **E.** Flowchart of siRNA curation and library assembly. Set 1 and Set 2 siRNAs were used in parallel to construct two independent single node (siNode) and node pair (siNodePair) libraries. For the siNode library, each siRNA pool consists of siRNAs targeting all paralogs within the gene node (the *RAF* siNode pool is illustrated as an example). For the siNodePair library, each siRNA pool consists of siRNAs targeting all paralogs within two gene nodes (the *RAF*+*AKT* siNodePair is illustrated as an example).

Fig. S2. Single node dependency analysis with Set 1 and Set 2 libraries.

- **A.** Cell viability data of single node knockdown by Set 1 vs Set 2 siRNA libraries in colorectal cancer cell lines. Cell viability was measured 5 days post siRNA transfection and was normalized to the siNeg control for the respective cell line.
- **B.** Correlation between Set 1 and Set 2 siNode library viability data.
- **C.** Outlier analysis for Set 1 vs. Set 2 siNode library concordance. For each siNode (*x*-axis), a z-score for the difference in viability by Set 1 and Set 2 siRNAs was calculated (*y*-axis). Outliers was identified using the ROUT analysis (Q = 1%). The HK node siRNAs were identified as an outlier (red).

Fig. S3. Correlation between single node dependency and *KRAS* dependency. Correlation plot of the viability of individual cell lines in response to siKRAS vs. siRAF (**A**), siRAL (**B**), siGLS (**C**), siMEK (**D**) and siERK (**E**). The correlation (R^2) between siKRAS and each siNode was calculated using data from the five *KRAS* mutant cell lines.

Fig. S4. Comparison of RAF, MEK and ERK node dependency in *KRAS* mutant cells.

- **A.** Western blot validation of target protein knockdown by the indicated siNode pools. Cell lysates was collected 5 days post siRNA transfection. Phospho-ERK1/2 (p-ERK1/2) was used as a readout for MAPK pathway activity.
- **B.** Quantification of phospho-ERK1/2 (p-ERK) levels in the western blots as shown in panel **A**. Comparable degree of p-ERK reduction was observed between Set 1 vs. Set 2 siRNAs for a given node, and between the siRAF, siMEK and siERK pools.
- **C.** Rescue of the cytotoxicity of Set 1 on-target *KRAS*, *RAF*, *MEK* and *ERK* siRNAs (left panel) by their corresponding C911 siRNAs (right panel).
- **D.** Unsupervised hierarchical clustering analysis of Set 1 siRNA cell viability data using Caco-2 as the sole *KRAS* WT control. Dendrogram branches involving siKRAS are highlighted in red. For each siNode, averaged differential dependency scores (DDS) and Pearson correlation coefficient (*r*) with siKRAS are listed.
- **E.** Top public single node dependency based on average Set 1 siRNA DDS using Caco-2 as the sole *KRAS* WT control. Bars represent the average DDS across five *KRAS* mutant cell lines.

Fig. S5. Paired-node dependency analysis with Set 1 and Set 2 libraries.

- **A.** Cell viability data of paired-node knockdown by Set 1 vs Set 2 siRNA libraries in colorectal cancer cell lines. Cell viability was measured 5 days post siRNA transfection and was normalized to the siNeg control for the respective cell line.
- **B.** Correlation between Set 1 and Set 2 siNodePair library viability data.
- **C.** Outlier analysis for Set 1 vs. Set 2 siNodePair library concordance. For each siNodePair (*x*-axis), a z-score for the difference in viability by Set 1 and Set 2 siRNAs was calculated (*y*-axis). Outliers was identified using the ROUT analysis (Q = 1%). Outlier siNodePair were colored red.

Fig. S6. Detailed view of selected node pair clusters highlighted in Figure 2A.

A. The Death cluster includes the siDeath control and most of BCL2-based node pairs. The RAF+PI3K and RAF+MEK node pairs also clustered here.

B. The PI3K cluster includes the majority of PI3K-based node pairs. Cell lines marked with * harbor mutations in *PIK3CA* or *PIK3CB* genes.

C. The MEK cluster includes the majority of MEK-based node pairs. The cell line SW48 (marked with *) harbor mutations in *MEK1* and is sensitive to MEK node knockdown.

D. The ERK cluster that are enriched for ERK-based node pairs.

Fig. S7. Comparison of RAF, MEK and ERK node pair dependency in *KRAS* mutant cells.

A. Scatter plot of DDS and *r* values for the 5 *KRAS* mutant cell lines from Set 1 siRNA data excluding the SW48 cell line. All node pairs involving the RAF, MEK and ERK nodes were highlighted.

B. Top RAF, MEK, and ERK-based node pairs based on DDS calculated from Set 1 siRNA data excluding the SW48 cell line. Viability of single node *RAF*, *MEK* and *ERK* knockdown is included for comparison. Bars represent the average DDS across five *KRAS* mutant cell lines and dots represent data points for individual cell lines.

Fig. S8. Top private node pair dependency for individual cell lines.

Node pair dependency was ranked based on cell line-specific DDS. siKRAS was included as a positive control. Notably, top node pair dependency typically includes the top single node dependency in the combination.

Fig. S9. Additional analysis of public node pair dependencies.

A. *KRAS* wild-type and mutant CRC and PDAC cell lines were transfected with siKRAS, siRAF node, and siNodePair combinations as indicated. Cell viability was determined 5 days post-transfection and normalized to siNeg control. Bars represent the average cell viability across 3 *KRAS* wild-type or 20 *KRAS* mutant cell lines and dots represent data points for individual cell lines (n.s., not significant; ** $p < 0.01$; *** $p < 0.001$).

B. Correlation plot of the viability of individual cell lines in response to siKRAS vs. siRAF node in CRC and PDAC cell lines. The correlation (R^2) was calculated using data from the 10 *KRAS* mutant cell lines.

C. Correlation plot of the viability of individual cell lines in response to siKRAS vs. siNodePair combinations as indicated in CRC and PDAC cell lines. The correlation (R^2) between siKRAS and each siNode was calculated using data from the 10 *KRAS* mutant cell lines. Cell line symbols are the same as panel B.

D. Rescue of the cytotoxicity of on-target siKRAS, siRAF node and siNodePair combinations by their corresponding C911 siRNAs pools.

Fig. S10. Toxicity evaluation of gene combination knockdown in immortalized normal cell lines.

A. Immortalized normal cell lines were transfected with siRNAs targeting individual gene paralogs as indicated. Cell viability was determined 4 days post-transfection.

B. Average DDS of CRC and PDAC cell lines in response to siKRAS and siRNA combinations targeting *RAF* paralogs. Bars represent the average DDS across 10 *KRAS* mutant cell lines and dots represent data points for individual cell lines (*** $p < 0.005$).

Fig. S11. Deconvolution of node pair dependencies to minimal gene paralog combinations.

A. Scatter plots showing the relationship between DDS and *r* metrics for all siRNA combinations.

B. Scatter plots showing the relationship between DDSn and *r* metrics for all siRNA combinations.

C. Scatter plots showing the relationship between DDS and DDSn metrics for all siRNA combinations.

D. Ranking of siRNA combinations based on DDS. siRNAs targeting *KRAS* and *RAF* paralogs were included for comparison. Bars represent the average DDS across 10 *KRAS* mutant cell lines and dots represent data points for individual cell lines. A heatmap for corresponding *r* and *p*-values (compared to *RAF* knockdown) are shown below the bar chart. Gene symbol abbreviations are the same as Figure 4A.

E. Ranking of siRNA combinations based on DDSn. siRNAs targeting *KRAS* and *RAF* paralogs were included for comparison. Bars represent the average DDSn across 10 *KRAS* mutant cell lines and dots represent data points for individual cell lines. A heatmap for corresponding *r* and *p*-values (compared to *RAF* knockdown) are shown below the bar chart. Gene symbol abbreviations are the same as Figure 4A.

Fig. S12. On-target validation of gene paralog siRNA combinations.

Rescue of the cytotoxicity of on-target siRNA combinations by their corresponding C911 siRNAs pools in the indicated cell lines (error bars represent S.D.).

Fig. S13. Knockdown validation of gene paralog siRNA combination.

- **A.** *KRAS* mutant HCT116 and *KRAS* WT Caco-2 CRC cells were transfected with various combinations of on-target siRNA combinations and their corresponding C911 siRNA combinations. Whole cell extracts were collected 5 days post-transfection and subjected to immunoblotting using antibodies against the targets and downstream proteins in the MAPK and autophagy pathways. FRA1 level in Caco-2 cells was not detectable (n.d.). Gene symbol abbreviations are the same as Figure 4A.
- **B.** Quantification of changes in protein levels from blots in panel A. Relative protein level is presented as log2 fold change compared to siNeg (n.d., non-detectable). Gene symbol abbreviations are the same as Figure 4A.

Fig. S14. RAC1 and ATG7 depletion sensitizes *KRAS* mutant cells towards MAPK pathway inhibitors.

KRAS mutant cancer cell lines HCT116 and MIA PaCa-2 and *KRAS* WT cancer cell line BxPC-3 were transfected with siRNAs against *RAC1* and/or *ATG7*. One day post transfection cells were treated with the RAF inhibitor RAF709 or the MEK inhibitor trametinib. Cell viability was determined 4 days later to obtain the dose response curves (error bars represent S.D.).

- **A.** RAF709 dose response curves.
- **B.** Trametinib dose response curves.

Fig. S15. Impact of *RAC1* and *ATG7* knockdown on cell cycle and cell death.

KRAS mutant (HCT116, MIA PaCa-2, and SW403) and WT (Caco-2 and SW48) cancer cell lines were transfected with siRAC1 or siATG7. Cell cycle and apoptosis status were analyzed 3 days post-transfection.

- **A.** Changes in G0/G1 viable cell populations by flow cytometry (** $p < 0.01$ vs. siNeg).
- **B.** Changes in sub-G1 dead cells by flow cytometry.
- **C.** Changes in caspase 3/7 activity in cells.

Fig. S16. A model of the cooperative role between RAF and autophagy in mediating *KRAS* oncogene addiction.

In *KRAS* WT cells, balanced signaling from WT RAS proteins to RAF paralogs leads to physiological proliferation. Co-depletion of BRAF, CRAF and ATG7 has relatively little impact on WT cell viability as ARAF is sufficient to mediate physiologic RAS signaling and autophagy is dispensable under nutrient replete conditions. In *KRAS* mutant cells, BRAF and CRAF are the critical onco-effectors for mutant KRAS, whereas autophagy serves as a protection mechanism against metabolic stress. Co-depletion of BRAF, CRAF and ATG7 results in both a reduction in proliferative and survival signal and a loss of protection against oncogenic stress, thus leading to enhanced cell cycle arrest and/or elevated apoptosis in *KRAS* mutant cells. This combination selectively targets both aspects of oncogene and non-oncogene addiction downstream of KRAS to preserve the therapeutic window for *KRAS* mutant cells.